



Physics-Based Method for the Removal of Spurious Resonant Frequencies in High-Frequency Force Balance Tests

Wei Cui, S.M.ASCE¹; and Luca Caracoglia, A.M.ASCE²

Abstract: The high-frequency force balance (HFFB) test is a widely used method for estimating lateral turbulent wind loads on tall buildings in a wind tunnel. The method relies on use of a highly accurate force sensor placed at the base of the tall building model to measure base forces and overturning moments. Because the turbulent wind load excitation is broadband, it is important to adequately design the connection detail between the model and the sensor. Accurate design is needed to avoid contaminating the measurement of the lateral wind loads by the potential spurious resonant effect, which is induced by flexibility in the connection detail. This design often relies on the experience of the wind tunnel modeler. On occasion, because of the limitations of test setup and environment, the connection detail between the building model and the HFFB force sensor may not be sufficiently stiff. Consequently, resonant response caused by the flexible connection may affect the power spectral density function of the measured wind loads. One of the methods to address this problem is to filter the HFFB output signal and to remove undesirable response within a specific frequency interval by conventional digital filter methods. However, this may cause the removal of important features of the wind loading. This paper presents a simple yet efficient method, based on classical dynamic theory, to eliminate the spurious effect. The method is applied to the “correction” of an experimental wind load spectrum. DOI: [10.1061/\(ASCE\)ST.1943-541X.0001414](https://doi.org/10.1061/(ASCE)ST.1943-541X.0001414). © 2015 American Society of Civil Engineers.

Author keywords: High-rise building; Wind tunnel; Power spectral density; Resonance vibration; Wind effect.

Introduction

High frequency force balance (HFFB) is a dynamic force measurement procedure often employed to record time series of the wind loading in a wind tunnel test. For more than thirty years, HFFB has been a very effective tool for estimating generalized wind forces on tall buildings with linear uncoupled mode shapes (Davenport and Tschanz 1981; Kareem and Cermak 1978; Tschanz and Davenport 1983; Reinholt and Kareem 1986; Boggs and Peterka 1989). The method consists of exposing a building model to a boundary-layer flow in a wind tunnel to replicate full-scale atmospheric wind conditions. However, deriving useful force information from the measured base reactions, needed to obtain an estimate of the structural response at full scale, is not straightforward and involves several pre-assumed conditions, such as linear mode shape. A simplified approach for correcting loads when the mode shapes of the real structure are not linear is presented by Holmes (1987). In Zhou et al. (2002), mode shapes are corrected according to an equivalent static wind load. Chen and Kareem (2005) proposed a framework to identify the distribution of spatiotemporally fluctuating wind loads on a building and to eliminate the need for mode shape corrections. Bernardini et al. (2013), from the perspective of performance-based wind engineering, proposed a method to include the uncertainties

arising from the lack of knowledge about the pressure field and to estimate any structural response parameter of interest.

Nevertheless, the frequency scale between the model and the full-scale structure may be large (by dynamic similarity). This requirement, combined with small turbulence scales in wind tunnels, may result in the need for sampling the output signal of the HFFB sensor at a rate of 200 samples per second or higher (e.g., for buildings with a geometric scale ratio of about 1:400 and tested at mean flow speed of approximately 10 m/s). Ideally, the natural frequency of the model setup should be at least two times (Nyquist frequency) the value of the highest frequency of interest (Stathopoulos and Baniotopoulos 2007). A typical plot of the power spectral density (PSD) of the cross-wind force on a rectangular-floor-plan building model (Tse et al. 2009b) is shown, as an example, in Fig. 1.

The peak of the PSD curves, influenced by wake-induced effects (Melbourne 1980), is of interest to researchers; also of interest is the “descending slope” at higher frequencies in the inertial subrange—for example, in the shaded region beyond $nB/U_H = 0.2$ in Fig. 1. Ideally, to satisfy the HFFB test requirement, the model’s first natural frequency should be at least twice the frequency of the rightmost point of the descending slope. However, this requirement may be realistically difficult to implement, especially for small-scale models (1:400 or smaller).

Fig. 2 shows the HFFB output data, obtained from measurements conducted on a tall building model in the small-scale wind tunnel at Northeastern University (NEU). This is an example in which interference due to the model’s resonant vibration is not negligible. The PSD curves of the cross-wind force are plotted on a log-log plane when the mean wind attack angles θ are 0° and 90° ; the frequency scale and PSD curves are normalized according to the model dimensions and mean wind speed. The experiment replicates the behavior of a prismatic tall building of base dimensions $B, D > B$, and height H in turbulent wind flow. The angle $\theta = 90^\circ$ refers to the flow perpendicular to the face of

¹Ph.D. Candidate, Dept. of Civil and Environmental Engineering, Northeastern Univ., 400 Snell Engineering Center, 360 Huntington Ave., Boston, MA 02115. E-mail: cui.we@husky.neu.edu

²Associate Professor, Dept. of Civil and Environmental Engineering, Northeastern Univ., 400 Snell Engineering Center, 360 Huntington Ave., Boston, MA 02115 (corresponding author). E-mail: lucac@coe.neu.edu

Note. This manuscript was submitted on October 18, 2014; approved on August 11, 2015; published online on September 10, 2015. Discussion period open until February 10, 2016; separate discussions must be submitted for individual papers. This paper is part of the *Journal of Structural Engineering*, © ASCE, ISSN 0733-9445/04015129(7)/\$25.00.

dimension B (shorter side). More details on the model setup are provided in the next section.

From the figure, a number of unexpected peaks can be seen in the region designated with the label “resonant vibration.” This is because both the cross-wind and the along-wind model setups suffer from resonant vibration triggered by turbulence in the oncoming flow. Modal coupling and two closely spaced frequencies, corresponding to the two fundamental modes of the HFFB setup, are noticeable for $\theta = 90^\circ$. These frequencies are closely spaced because of geometric and mass symmetry in the setup, influenced by small imperfections that are unavoidable in a typical experimental setting.

Fig. 2 clearly illustrates the motivation for this study. In this work, several methods are examined to eliminate the undesired

peaks caused by resonant vibration and to restore an “uncorrupted” PSD curve. A physics-based method is also proposed, using a simplified cantilever beam model with lumped mass at the top of the cantilever, to approximate the dynamics of the flexible components in the experimental setup—that is, the connection detail between the force sensor and the building model. Both single-degree-of-freedom (DOF) and two-DOF reduced-order models are considered. It is demonstrated that the the single-DOF model can efficiently remove one spurious resonant peak from the force PSD curve at a time, whereas the two-DOF dynamic model can remove two coupled-mode spurious peaks from the force PSD in cross-wind directions.

Experimental Setup

Wind tunnel tests were conducted in NEU’s small-scale closed-circuit wind tunnel, shown in Fig. 3(a). The dimensions of the test chamber are 560×560 mm, and the maximum flow speed in the test chamber is approximately 20 m/s. As a first approximation of a boundary-layer wind simulation for high-rise buildings, turbulence is generated in the wind tunnel by a grid; unfortunately, boundary-layer flow cannot be easily simulated in this small facility. The width of each rectangular-section bar of the grid is 20 mm; the depth is less than 5 mm; and the center-to-center

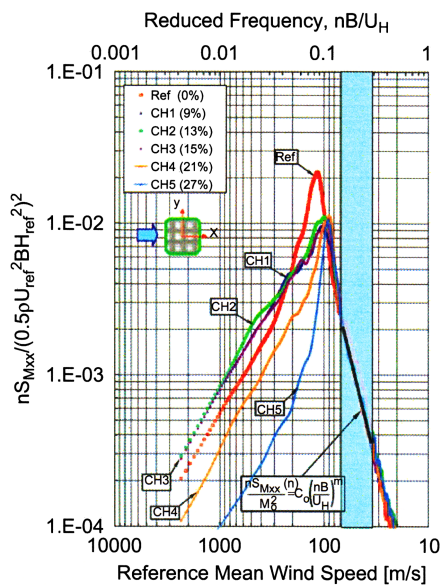


Fig. 1. Typical power spectral density (PSD) plot of cross-wind forces, extracted by HFFB in a wind tunnel experiment (n = frequency; U_H = mean wind speed at model roof height H ; B = reference geometric dimensions; ρ = air density) (image taken from Tse et al. 2009b, reproduced with permission from Elsevier.)

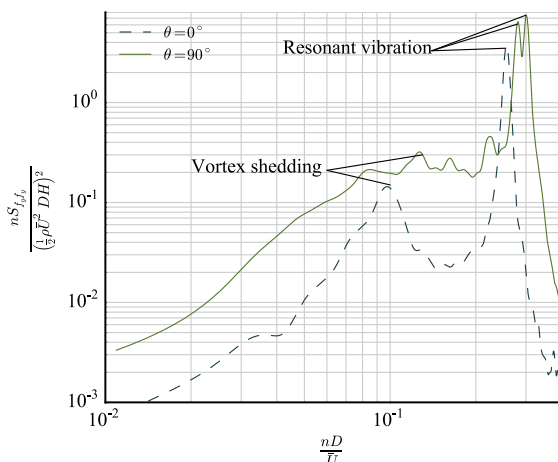
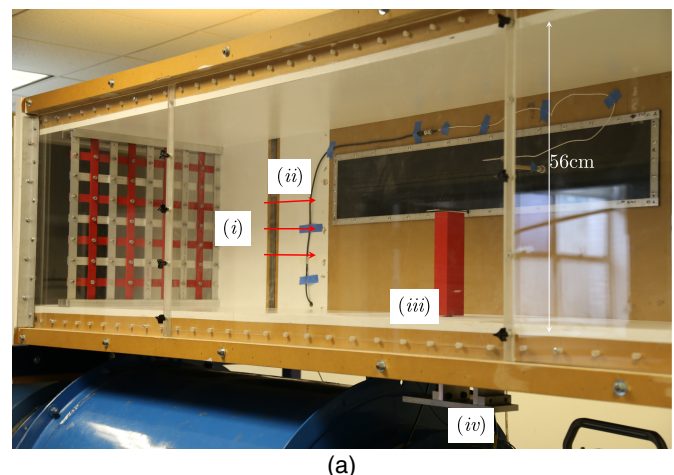
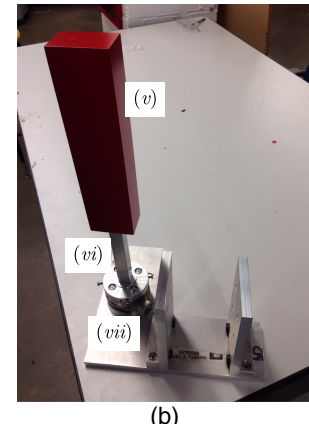


Fig. 2. Example of normalized cross-wind force PSD, measured by HFFB and contaminated by the model’s resonant interference (n = frequency; \bar{U} = mean wind speed at model roof height H ; D = reference dimensions)



(a)



(b)

Fig. 3. Experimental setup in NEU’s wind tunnel: (a) chamber: (i) turbulence grid; (ii) flow direction; (iii) building model; (iv) HFFB; (b) HFFB sensor: (v) building model; (vi) flexible connection; (vii) HFFB

gap between each bar is 40 mm. The solidity ratio of the grid is 0.333. Along-wind turbulence intensity at the location of the model, approximately 1.32 m downstream from the grid, is approximately 0.14 [Fig. 3(a)]; the length scale of turbulence is approximately 50 mm. The model represents, at a 1:750 scale, the characteristics of the Commonwealth Advisory Aeronautical Research Council (CAARC) standard building (Melbourne 1980). Model dimensions are: rectangular base of width $D = 60$ mm, depth $B = 40$ mm, and height $H = 284$ mm. Consequently, wind tunnel blockage is still acceptable (4%). For the purpose of illustrating the applicability of the proposed method, tests are carried out at $\theta = \{0^\circ, 90^\circ\}$ and uniform mean flow speed \bar{U} variable between 8 and 10 m/s.

To avoid resonant effects in the HFFB setup at low frequencies, the mass of the model and connection detail were designed to be as small as possible. The mass of the building, made of hard hollow plastic, is approximately equal to 300 g [Fig. 3(a)]. The model is connected to the HFFB through a hollow square aluminum tube, whose dimensions are $19 \times 19 \times 6.4$ mm [Fig. 3(b)]. The base force sensor (HFFB) is a six-axis Gamma-type force balance (ATI Industrial Automation, Apex, North Carolina); it is mounted on a very thick aluminum plate and placed beneath the chamber to acquire the force data [Fig. 3(a)]. Because of the previously described imperfections in the setup, two coupled spurious resonant response peaks in the PSD of the wind force are recorded at the base of the model at a reduced frequency close to 0.4 (Fig. 2). The non-negligible length of the connecting aluminum bar [Fig. 3(b)] is believed to be responsible for the appearance of the spurious peaks in this frequency range. Even though this slender connection detail is required by clearance restrictions in the NEU's wind tunnel, it is not unusual to find a similar setup in other, larger facilities.

Normally, elimination of spurious resonance can be addressed through standard postprocessing of HFFB data, for example using signal filtering to remove unwanted peaks from the PSD curve. In the following sections, the standard signal-filtering method is first reviewed. Then the proposed method, based on classical structural dynamic theory, is introduced and compared to standard signal filtering.

Standard Digital Signal Filtering

The Butterworth filter (Butterworth 1930) has been applied to data processing for many decades; it is a useful technique for removing undesirable information from the time series of the base force, recorded through the HFFB. Typically, a band-pass filter may be used (normally “low-pass” with a cut-off frequency of $0.4 \sim 100$ Hz) to remove the high-frequency components of a signal, which are usually considered unimportant and associated with ambient or instrumental noise (Steckley et al. 1992). Similarly, it is plausible to use a Butterworth band-stop filter to remove unwanted peaks in the HFFB output force records.

The dash-dot-dot line in Fig. 4 is obtained by applying a Butterworth band-stop filter to a typical record of the cross-wind base force at mean flow angle $\theta = 0^\circ$ as measured by NEU's HFFB (Fig. 2). The sampling frequency of the HFFB records is set to 1,000 Hz; a digital band-pass filter of order 3 between the frequencies of 55 and 75 Hz is employed. The results for $\theta = 90^\circ$ are omitted for the sake of brevity. One important side effect is that not only the resonant response but also important information related to the turbulent background wind load is removed. Therefore, the PSD curve in Fig. 4 in the $n/\bar{U}D$ region, where the band-stop filter is applied, rapidly reduces to almost zero.

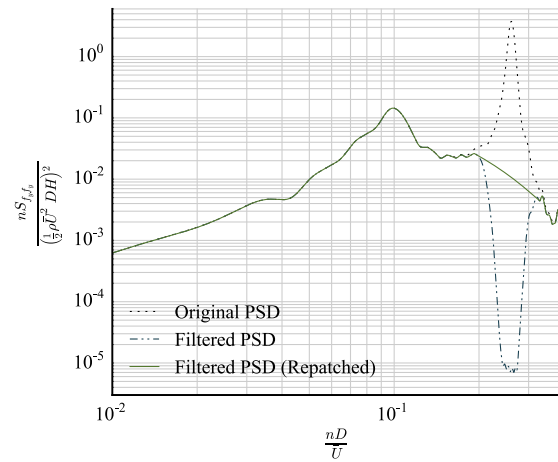


Fig. 4. Digital signal filtering to remove spurious resonant peaks of cross-wind force PSD; mean incident flow angle $\theta = 0^\circ$

To restore the trend in the PSD curve after application of the band-stop filter, a “straight line” on the log-log plane is occasionally used by the wind tunnel modeler to fill the “dip” caused by the filter, as shown by the solid line in Fig. 4. The use of this empirical correction may be justified because wind tunnel test experience indicates that this phenomenon is usually recorded in a region of the wind force PSD, generated by flow turbulence in the inertial subrange—that is, away from wake-induced effects due to vortex shedding (refer to the straight line on the log-log scale plot in Fig. 1 beyond $nD/\bar{U} = 0.2$). More sophisticated filtering techniques may be used, but the principle of adequate signal reconstruction and the need for preserving the turbulence features in the region where the spurious resonant peaks occur still remain. The use of digital filtering has two disadvantages: the band-stop upper and lower frequencies are selected manually; also, the solid line in Fig. 4, correcting the dip produced by the band-stop filter, may not represent the physical PSD trend because the slope is influenced by the choice of upper and lower filter frequencies.

Physics-Based Method

Single-DOF Reduced-Order HFFB Dynamic Model

Because most flexibility in the test setup is associated with the connection element between the model and the force balance [aluminum tube in Fig. 3(b)], and because the building model is practically rigid, the dynamics of the HFFB measurement system can be represented by a “spring-mass-damping” model in its simplest form. This model is shown schematically in Fig. 5. The hypothesis of concentrated mass at the top of the connection element is based on the observation that fundamental-mode lateral vibration of the flexible balance is mainly associated with low-amplitude translation motion. The derivation in the following sections employs, as physical DOF, the lateral translation of the base point only. This point-mass translation can be considered a combination of the effects of system translation and rotation. It can be shown that the derivation is also valid in generalized terms (modal expansion) even when dynamic rotation effects and inertia are included. In any case, the method works since the actual values of the mass or inertia are not needed and therefore are indirectly embedded in the equations as generalized terms in a modal expansion.

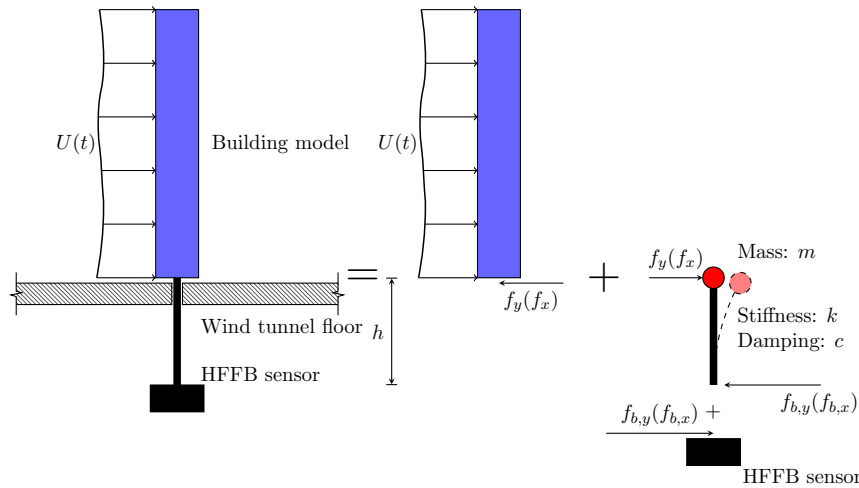


Fig. 5. Schematic of single-DOF equivalent model (m = the “lumped mass” of the model; the HFFB sensor records the force transferred to the fixed base)

If the x (along-wind) and y (cross-wind) loads and “responses” (i.e., the imperceptible sway motion at the base of the model) are assumed to be uncoupled, one independent HFFB reduced-order model can be built in each direction. For example, the equivalent equation of motion of the dynamic model in the cross-wind direction is, in the time domain

$$m\ddot{y}(t) + c\dot{y}(t) + ky(t) = f_y(t) \quad (1)$$

where f_y = lateral wind load at the base of the building (or equivalent base shear) that needs to be identified.

In Eq. (1) and in a later section, the term *along-wind* is used to designate the force and vibration in the direction corresponding to the mean flow direction coincident with the longitudinal axis of the tunnel chamber, whereas the cross-wind terms are horizontal-transverse. The over-dot symbol is employed in Eq. (1) for the derivative with respect to time t . The equation also assumes that, because of very small model velocity magnitude and high vibration frequency, aero-elastic interaction is negligible in the flexible HFFB system; therefore, the forcing term $f_y(t)$ in Eq. (1) is exclusively composed of external excitation forces, either buffeting or wake-induced. After Fourier transformation, with $\iota = \sqrt{-1}$ and ω generic angular frequency, Eq. (1) becomes

$$(-m\omega^2 + \iota c\omega + k)\hat{y}(\omega) = \hat{f}_y(\omega) \quad (2)$$

After substituting the natural angular frequency $\omega_0 = \sqrt{k/m}$ and the damping ratio $\xi = c/2m\omega_0$, which simulates mechanical damping in the HFFB system, Eq. (2) can be rewritten as

$$\left(-\frac{\omega^2}{\omega_0^2} + 2\iota\xi\frac{\omega}{\omega_0} + 1\right)\hat{f}_{b,y}(\omega) = \hat{f}_y(\omega) \quad (3)$$

From Eq. (3) the relationship between the PSD of the lateral force $S_{f_yf_y}$ (to be found) and the actual spectrum measured by the HFFB sensor $S_{f_{b,y}f_{b,y}}$ can be determined, in the cross-wind direction for example, as

$$S_{f_yf_y} = S_{f_{b,y}f_{b,y}}H_{tr} \quad (4)$$

in which

$$H_{tr}(\omega|\omega_0) = \left[\left(1 - \frac{\omega^2}{\omega_0^2} \right)^2 + 4\xi^2 \frac{\omega^2}{\omega_0^2} \right] \quad (5)$$

The advantage of Eq. (4) is that the mass m and the generalized stiffness of the setup are not directly included; moreover, the angular frequency ω can be replaced by frequency n or by reduced frequency nD/\bar{U} . Two equivalent equations can also be derived for the along-wind direction (x); derivation is omitted for the sake of brevity.

Preliminary “wind-off” tests in NEU’s wind tunnel (impact and free vibration tests in each primary direction) are carried out to determine the only term that is needed by Eq. (5), ξ . It is found that the model’s damping ratio (Fig. 5) is $\xi = 0.94\%$. The peak frequency in the PSD curve can be found by inspection of Fig. 2 in the case of cross-wind vibration; this corresponds to reduced frequency $n_0D/\bar{U} = 0.261$ and dimensional frequency $n_0 = 67.6$ Hz. The frequency transfer function $H_{tr}(nD/\bar{U})|_{n_0}$ is plotted in Fig. 6.

The post-multiplication between $S_{f_{b,y}f_{b,y}}$ (PSD of the force recorded by the HFFB sensor) and the transfer function $H_{tr}(nD/\bar{U})|_{n_0}$ yields the PSD of the equivalent force at the top of the connection element (hollow aluminum bar) $S_{f_yf_y}$, which

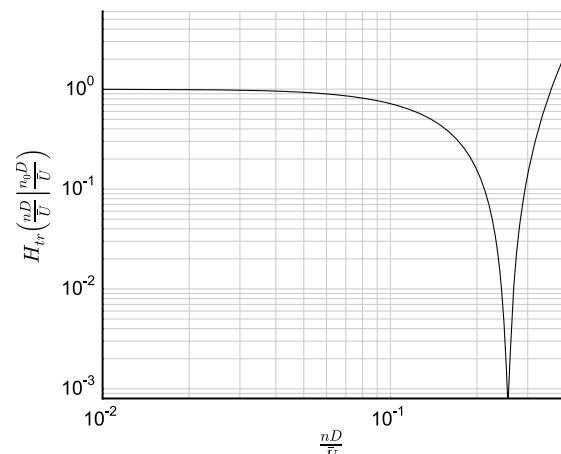


Fig. 6. Dynamic transfer function $H_{tr}(nD/\bar{U})$ applied to cross-wind direction force data

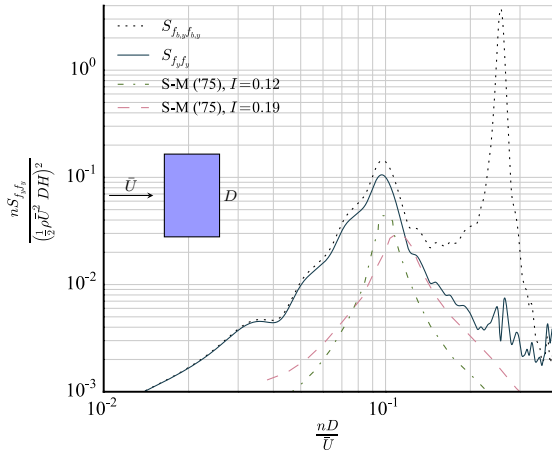


Fig. 7. Cross-wind force PSD after removal of resonance peaks by the single-DOF method; mean flow incident angle $\theta = 0^\circ$ [S-M ('75) indicates experimental results reproduced from Saunders and Melbourne (1975) at various turbulence intensities I .]

is the desired and uncontaminated force. This quantity is shown as a dotted line in Fig. 7 for the cross-wind force PSD when $\theta = 0^\circ$.

The solid line in Fig. 7 is the uncontaminated cross-wind PSD derived using the proposed method. The spurious resonant PSD is almost removed, but small residual fluctuations still exist because of an imperfect setup with coupled-mode response.

In Fig. 7, the PSD test results from NEU's experiments with turbulence intensity $I = 0.14$ are compared to the PSD curves experimentally found by Saunders and Melbourne (1975). These researchers conducted their tests on the same building model at 1:400 geometric scale in a simulated boundary-layer wind and power-law shear profile with exponent 0.21 (low-intensity profile, turbulence intensity $I = 0.12$) and exponent 0.37 (high-intensity profile with $I = 0.19$). Their PSD curves were also normalized with respect to the mean wind speed at the model's rooftop. The PSD curve obtained at NEU had the same peak at the vortex-shedding frequency compared with the PSD curves in Saunders and Melbourne (1975), with $I = 0.12$. However, NEU's PSD values at various frequencies were 3–5 times larger. The reason for this difference is that uniform flow is used at NEU, resulting in an overall increase in loads compared to the shear flow used by Saunders and Melbourne (1975). Moreover, their turbulence intensities decreased along the height of the model, whereas NEU's ones were approximately constant. Despite all the differences, the overall PSD results are acceptable; it must also be observed that the main objective of this work is examination of the physics-based method for removing the spurious resonant effect, successfully achieved as shown in Fig. 7.

When the mean flow incident angle is $\theta = 90^\circ$ (Fig. 8) and because of the previously mentioned geometry and mass imperfections, the cross-wind forces are coupled with the along-wind forces in the HFFB dynamic model. As a result, there are two peaks in the original cross-wind force PSD. The method described in Eqs. (1)–(5) cannot completely eliminate the second peak as it does with the first peak. Refer to the dash-dot-dot line in Fig. 8, which shows that one of the two peaks is reduced but not fully eliminated whereas the second one is unsuccessfully overfiltered.

To eliminate this effect, a “pseudo-2D” reduced-order model and method are introduced to remove both peaks in the PSD curve. This method combines $H_{tr}(nD/\bar{U}|n_{0,1}D/\bar{U})$ for cross-wind vibration and $H_{tr}(nD/\bar{U}|n_{0,2}D/\bar{U})$ for along-wind fundamental-mode

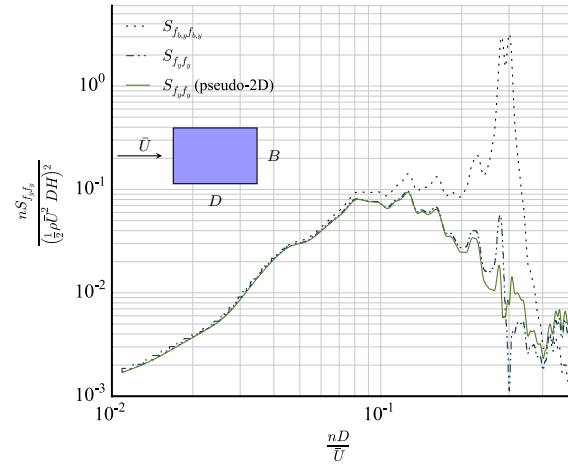


Fig. 8. Cross-wind force PSD after removal of resonance peaks through single-DOF method; mean flow incident angle $\theta = 90^\circ$

vibration (with $n_{0,1} = n_0$ Hz and $n_{0,2} = 63.3$ Hz); the geometric average between the two transfer functions (solid line in Fig. 9) is used. The PSD of the force at the top of the connection bar is

$$S_{f_y f_y} \approx \sqrt{H_{tr}(nD/\bar{U}|n_{0,1}D/\bar{U})H_{tr}(nD/\bar{U}|n_{0,2}D/\bar{U})}$$

This function is plotted as a solid line in Fig. 8. The pseudo-2D method can reduce both peaks from a practical point of view. However, it cannot correctly reproduce the physical coupling effect between along-wind and cross-wind generalized vibration in the dynamic HFFB system.

Two-DOF Reduced-Order HFFB Dynamic Model

The two-DOF method takes into account the coupling effect between along-wind and cross-wind generalized vibration. It uses the multi-DOF random vibration theory with simplified mass, stiffness distribution, and mechanical damping characteristics. The equation of motion in the time domain is

$$\ddot{\mathbf{M}} + \mathbf{C}\dot{\mathbf{d}} + \mathbf{K}\mathbf{d} = \mathbf{f} \quad (6)$$

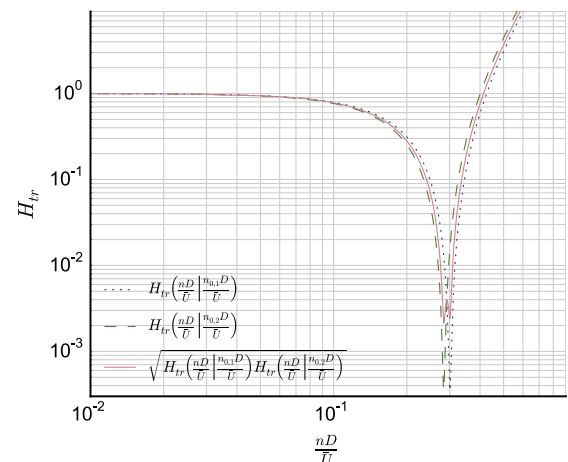


Fig. 9. Dynamic transfer function $H_{tr}(nD/\bar{U})$ applied to cross-wind direction force data when $\theta = 90^\circ$

in which

$$\mathbf{d} = \begin{Bmatrix} x \\ y \end{Bmatrix}, \quad \mathbf{f} = \begin{Bmatrix} f_x \\ f_y \end{Bmatrix}, \quad \mathbf{M} = m \begin{bmatrix} 1 & 0 \\ 0 & 1 \end{bmatrix} = m\mathbf{I}_{2 \times 2},$$

$$\mathbf{C} = c\mathbf{I}_{2 \times 2}, \quad \mathbf{K} = k \begin{bmatrix} 1 & \alpha \\ \alpha & 1 \end{bmatrix} \quad (7)$$

Because the connection element is approximately symmetric [square aluminum bar in Fig. 3(b)], it is reasonable to assume that mass and damping along the element are perfectly symmetric as in Eq. (6) and the imperfection can be modeled using a stiffness matrix \mathbf{K} with nonzero off-diagonal elements αk in Eq. (7). After Fourier transformation, Eq. (6) becomes

$$(-\mathbf{M}\omega^2 + \mathbf{C}\omega + \mathbf{K})\mathbf{d}(\omega) = \mathbf{f}(\omega) \quad (8)$$

The substitution of $\mathbf{d}(\omega) = \mathbf{K}^{-1}\mathbf{f}_b(\omega)$ in Eq. (8) yields

$$(-\mathbf{M}\mathbf{K}^{-1}\omega^2 + \mathbf{C}\mathbf{K}^{-1}\omega + \mathbf{I}_{2 \times 2})\mathbf{f}_b(\omega) = \mathbf{f}(\omega) \quad (9)$$

The angular natural frequencies in Eq. (6) are the eigenvalues of the homogeneous matrix problem associated with \mathbf{K} and \mathbf{M} ; they are

$$\omega_{0,1} = \omega_0\sqrt{1+\alpha}, \quad \omega_{0,2} = \omega_0\sqrt{1-\alpha} \quad (10)$$

in which $\omega_0 = \sqrt{k/m}$ is a reference “median” between $\omega_{0,1}$ and $\omega_{0,2}$.

The scalar damping coefficient c in the matrix \mathbf{C} can similarly be expressed as $2\xi m\omega_0$, and Eq. (6) can consequently be simplified as

$$\left(-\mathbf{A}^{-1}\frac{\omega^2}{\omega_0^2} + \mathbf{A}^{-1}2\xi\frac{\omega}{\omega_0} + \mathbf{I}_{2 \times 2} \right) \mathbf{f}_b(\omega) = \mathbf{f}(\omega) \quad (11)$$

in which $\mathbf{A} = \begin{bmatrix} 1 & \alpha \\ \alpha & 1 \end{bmatrix}$. As in Eq. (4), ω in Eq. (11) can easily be replaced by natural frequency n or reduced frequency. In Eq. (6), $\omega_{0,1}$ and $\omega_{0,2}$ can be determined by inspection of the graphs in the original force PSD in Fig. 2 or Fig. 8.

From Eq. (11), the cross-PSD matrix of the lateral wind force components f_x and f_y at the top of the connection element (i.e., the generalized base forces needed for wind load analysis) can be obtained from the cross-PSD matrix of the forces $f_{b,x}$ and $f_{b,y}$ recorded by the HFFB sensor as

$$\begin{bmatrix} S_{f_x f_x} & S_{f_x f_y} \\ S_{f_y f_x} & S_{f_y f_y} \end{bmatrix} = \mathbf{H} \begin{bmatrix} S_{f_{b,x} f_{b,x}} & S_{f_{b,x} f_{b,y}} \\ S_{f_{b,y} f_{b,x}} & S_{f_{b,y} f_{b,y}} \end{bmatrix} \mathbf{H}^{*,T} = \mathbf{H} \mathbf{S}_{f_b, f_b} \mathbf{H}^{*,T} \quad (12)$$

where $\mathbf{H} = [-\mathbf{A}^{-1}\omega^2/\omega_0^2 + \mathbf{A}^{-1}2\xi(\omega/\omega_0) + \mathbf{I}_{2 \times 2}]$; and $\mathbf{H}^{*,T}$ = transpose and conjugate of the matrix \mathbf{H} .

In the wind tunnel test at NEU, the matrix \mathbf{S}_{f_b, f_b} is calculated from the time series of $f_{b,x}$ and $f_{b,y}$ recorded by the HFFB sensor. Both PSDs of the forces $f_{b,x}$ and $f_{b,y}$ can be derived from Eq. (12); the cross-wind force is shown in Fig. 10.

The solid line in Fig. 10 demonstrates that the resonant response effect, caused by the coupled interaction between balance and wind force, can be practically eliminated using the two-DOF method. A small residual in the spurious peaks after application of the method is unavoidable because of nonuniformity and nonsymmetry in the

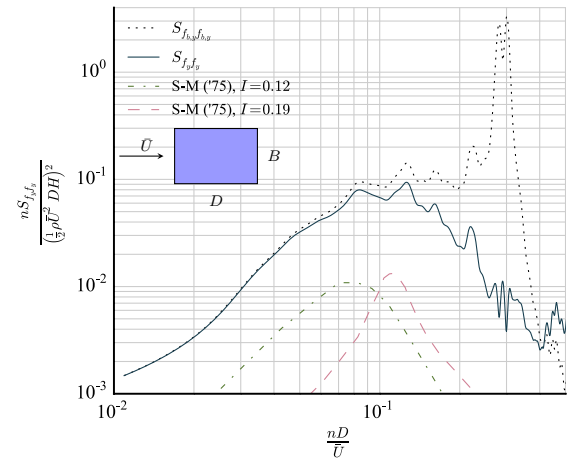


Fig. 10. Cross-wind force PSD after removal of resonance peaks by the two-DOF method; mean flow incident angle $\theta = 90^\circ$ [S-M ('75) indicate experimental results reproduced from Saunders and Melbourne (1975) at various turbulence intensities I .]

mass and damping distribution, which are not considered by the method.

NEU's PSD curve at the wind angle $\theta = 90^\circ$ is compared to Saunders and Melbourne's (1975) PSD results in Fig. 10. The comparison shows that the PSD curve measured in NEU's wind tunnel correctly identifies the broadband effects of vortex shedding; as before, larger PSD values are observed because of the absence of a shear layer profile with nonhomogeneous mean wind and turbulence flow.

Concluding Remarks

This paper describes two methods for removing spurious resonant peaks from HFFB wind tunnel measurements due to imperfections between the base force sensor and the building model.

The first method is derived from single-DOF random vibration theory and uses the transfer function $H_{tr}(\omega|\omega_0)$ in Eq. (5) to restore the PSD of the force f_y or f_x at the top of HFFB connection element (i.e., the base of the tested model) for a mean wind incident angle $\theta = 0^\circ$. For $\theta = 90^\circ$, another spurious resonant peak emerges because of imperfect symmetry. The single-DOF method can exclusively remove one frequency peak, so the following function is first used:

$$\sqrt{H_{tr}(nD/\bar{U}|n_{0,1}D/\bar{U})H_{tr}(nD/\bar{U}|n_{0,2}D/\bar{U})}$$

This function, combining the H_{tr} functions for two independent peaks, can partially eliminate the spurious peaks with coupling.

To overcome the limitations of the single-DOF method, a two-DOF formulation of the coupled dynamic system, replicating the flexible wind tunnel balance, is proposed. This formulation can effectively remove the two coupled resonant responses in both directions.

This work suggests that, in comparison with standard digital signal filtering, a physics-based method is more suitable to solving the problem caused by flexible HFFB connections because it relies on physical and theoretical modeling rather than empirical correction. It is anticipated that the proposed method may also be applied to the estimation of generalized wind forces on tall building models with nonlinear mode shapes (Tse et al. 2009a; Cluni et al. 2011).

Acknowledgments

Mr. Kurt Braun, Department of Civil and Environmental Engineering of NEU, is gratefully acknowledged for fabrication of the wind tunnel setup and for assistance during experiments. Mr. Jonathan Doughty, Department of Mechanical and Industrial Engineering of NEU, is acknowledged for 3D printing and model fabrication. Messrs. David Abati and Darren Vokes of NEU's Carpentry Department are gratefully acknowledged for the construction and assembly of the test chamber. Professor Jerome F. Hajjar and the Department of Civil and Environmental Engineering are gratefully acknowledged for their collaboration with the sensor equipment. Finally, the authors would like to thank the Department of Mechanical and Industrial Engineering of NEU for the shared use of wind tunnel facility. This paper is based on work supported by the National Science Foundation (NSF) of the United States under CAREER Award CMMI-0844977. Any opinions, findings and conclusions or recommendations are those of the authors and do not necessarily reflect the views of the NSF.

References

- Bernardini, E., Spence, S. M., and Kareem, A. (2013). "A probabilistic approach for the full response estimation of tall buildings with 3d modes using the HFFB." *Struct. Saf.*, **44**, 91–101.
- Boggs, D., and Peterka, J. (1989). "Aerodynamic model tests of tall buildings." *J. Eng. Mech.*, **10.1061/(ASCE)0733-9399(1989)115:3(618)**, 618–635.
- Butterworth, S. (1930). "On the theory of filter amplifiers." *Exp. Wireless Wireless Eng.*, **7**, 536–541.
- Chen, X., and Kareem, A. (2005). "Validity of wind load distribution based on high frequency force balance measurements." *J. Struct. Eng.*, **10.1061/(ASCE)0733-9445(2005)131:6(984)**, 984–987.
- Cluni, F., Gusella, V., Spence, S., and Bartoli, G. (2011). "Wind action on regular and irregular tall buildings: Higher order moment statistical analysis by HFFB and SMPSS measurements." *J. Wind Eng. Ind. Aerodyn.*, **99(6–7)**, 682–690.
- Davenport, A. G., and Tschanz, T. (1981). "The response of tall buildings to wind." *Proc., 4th U.S. National Conf. on Wind Engineering Research*, National Science Foundation Wind Engineering Research Council and the Univ. of Washington, Seattle, Washington.
- Holmes, J. D. (1987). "Mode shape corrections for dynamic response to wind." *Eng. Struct.*, **9(3)**, 210–212.
- Kareem, A., and Cermak, J. (1978). "Wind tunnel simulation of wind-structure interactions." *Proc., 24th Int. Instrumentation Symp.*, ISA, Albuquerque, New Mexico.
- Melbourne, W. (1980). "Comparison of measurements on the CAARC standard tall building model in simulated model wind flows." *J. Wind Eng. Ind. Aerodyn.*, **6(1)**, 73–88.
- Reinhold, T. A., and Kareem, A. (1986). "Wind loads and building response predictions using force balance techniques." *Dynamic response of structures*, G. C. Hart and R. B. Nelson, eds., ASCE, Reston, VA, 390–397.
- Saunders, J., and Melbourne, W. (1975). "Tall rectangular building response to cross-wind excitation." *Proc., 4th Int. Conf. on Wind Effects on Buildings and Structures*, Cambridge University Press, London, 369–380.
- Stathopoulos, T., and Baniotopoulos, C. C. (2007). *Wind effects on buildings and design of wind-sensitive structures*, Springer, Vienna, Austria.
- Steckley, A., Accardo, M., Gamble, S. L., and Irwin, P. A. (1992). "The use of integrated pressures to determine overall wind-induced response." *J. Wind Eng. Ind. Aerodyn.*, **42(1–3)**, 1023–1034.
- Tschanz, T., and Davenport, A. (1983). "The base balance technique for the determination of dynamic wind loads." *J. Wind Eng. Ind. Aerodyn.*, **13(1–3)**, 429–439.
- Tse, K., Hitchcock, P., and Kwok, K. (2009a). "Mode shape linearization for HFBB analysis of wind-excited complex tall buildings." *Eng. Struct.*, **31(3)**, 675–685.
- Tse, K., Hitchcock, P., Kwok, K., Thepmongkorn, S., and Chan, C. (2009b). "Economic perspectives of aerodynamic treatments of square tall buildings." *J. Wind Eng. Ind. Aerodyn.*, **97(9–10)**, 455–467.
- Zhou, Y., Kareem, A., and Gu, M. (2002). "Mode shape corrections for wind load effects." *J. Eng. Mech.*, **10.1061/(ASCE)0733-9399(2002)128:1(15)**, 15–23.